



HAL
open science

Deformation estimation of an earth dam and its relation with local earthquakes, by exploiting multitemporal synthetic aperture radar interferometry: Mornos dam case (Central Greece)

Spiros Neokosmidis, Panagiotis Elias, Issaak Parcharidis, Pierre Briole

► To cite this version:

Spiros Neokosmidis, Panagiotis Elias, Issaak Parcharidis, Pierre Briole. Deformation estimation of an earth dam and its relation with local earthquakes, by exploiting multitemporal synthetic aperture radar interferometry: Mornos dam case (Central Greece). *Journal of applied remote sensing*, 2016, 10 (2), pp.026010. 10.1117/1.JRS.10.026010 . hal-04270306

HAL Id: hal-04270306

<https://hal.science/hal-04270306v1>

Submitted on 4 Nov 2023

HAL is a multi-disciplinary open access archive for the deposit and dissemination of scientific research documents, whether they are published or not. The documents may come from teaching and research institutions in France or abroad, or from public or private research centers.

L'archive ouverte pluridisciplinaire **HAL**, est destinée au dépôt et à la diffusion de documents scientifiques de niveau recherche, publiés ou non, émanant des établissements d'enseignement et de recherche français ou étrangers, des laboratoires publics ou privés.

Deformation estimation of an earth dam and its relation with local earthquakes, by exploiting multitemporal synthetic aperture radar interferometry: Mornos dam case (Central Greece)

Spiros Neokosmidis,^{a,*} Panagiotis Elias,^b Issaak Parcharidis,^a and Pierre Briole^c

^aHarokopio University of Athens, Department of Geography, El. Venizelou 70, Athens 17672, Greece

^bNational Observatory of Athens, Institute of Astronomy, Astrophysics, Space Applications and Remote Sensing, I. Metaxa & Vas. Pavlou, Penteli 152 36, Greece

^cCNRS, Ecole Normale Supérieure, Department of Geosciences, Paris 75231, France

Abstract. Monitoring dam performance is a critical parameter in maintaining a safe dam. Safety concerns include seepage, internal erosion, and seismic issues in the case that the dam is located in high seismic hazard areas. Seismic considerations for dam safety among others includes the expected dam's performance during seismic events. The scope of this research work concerns the capability to record potential deformation on the Mornos earth dam (central Greece) induced by major earthquake events that occurred in the broader area. For this purpose, a hybrid interferometry synthetic aperture radar (InSAR) method was applied using elements of conventional differential InSAR, short baseline interferometry approaches, and persistent scatterers interferometry. A time series of ascending and descending acquisitions of active microwave instrument/ERS-1 and 2 and advanced synthetic aperture radar/ENVISAT scenes covering the period from 1993 to 2010 were interferometrically combined. Five very strong seismic events with epicenters close to the dam, at the same period, were considered as potential sources of deformation. The lake's water surface elevation was also considered as an additional factor of induced deformation. Results show a maximum deformation rate of ~ 10 cm along the line of sight for the whole period. Although the observed deformation appears to be due to changes in water level following a particular pattern, this is interrupted over time, and these interruptions coincide in time with specific seismic events. © 2016 Society of Photo-Optical Instrumentation Engineers (SPIE) [DOI: 10.1117/1.JRS.10.026010]

Keywords: infrastructure monitoring; synthetic aperture radar interferometry and seismic hazard.

Paper 15644 received Sep. 16, 2015; accepted for publication Mar. 18, 2016; published online Apr. 25, 2016.

1 Introduction

Dams are multipurpose projects having significant social and economic impact, such as flood control, irrigation, water supply, and electricity production. Monitoring a dam plays an essential role in its management and operation, especially for unsafe conditions or problems that require appropriate corrective measures at the early stages. Possible failure can cause great disasters with enormous social, economic, and ecological costs.^{1,2} The kinematic behavior is directly related to the probability of its failure; for this reason, its monitoring is of particular importance. During the last decades, remote sensing techniques (e.g., laser scanner, differential interferometry) came to complement the methods for measuring the displacement of infrastructures with *in situ*

*Address all correspondence to: Spiros Neokosmidis, E-mail: s.neokosmidis@noa.gr

instruments such as GPS. Among these techniques, the differential interferometry synthetic aperture radar (DInSAR) is used to measure the micromovements with millimeter precision. In the previous years, in order to study the structural deformation of Mornos Dam, four survey campaigns from 2002 to 2004 were carried out.³ In this paper, the study of the surface deformation occurring in the region of the Mornos Dam and the dam itself, which is based on the application of differential radar interferometry and singular value decomposition (SVD) methodologies, is presented. Our study is focused on the period from 1992 to 2000 and 2003 to 2010, exploiting active microwave instrument (AMI)/ERS-1 and 2 and advanced synthetic aperture radar (ASAR)/ENVISAT, ascending and descending acquisitions. The availability of these ascending/descending data sets allows us to discriminate the vertical and east–west displacement components as well. The importance of the Mornos Dam, being the provider of a reservoir of potable water to the greater metropolitan area of Athens, supporting 4.5 million people daily, along with the fact that it is located in a seismically active area was the motivation of the current study.

2 Test Site

2.1 Geological Setting

The Mornos River, with a total length of 77 km, crosses the central mainland Greece. The sources are located on the southern slopes of Oiti, descending toward the south draining the basin located between Giona, Vardousion, and Lidoriki, and flowing into the limits of the Gulf of Corinth and Patras, west of Nafpaktos.

The artificial lake of Mornos (Fig. 1), 7 km west of Lidoriki, was built to meet the ever-growing needs for water supply of Athens. The total surface of the lake, which is the average level, is ~ 15.5 km², making it the ninth largest artificial lake in Greece.

The main geological formations of the area belong to the external Hellenides, namely the Parnassos-Giona, Vardousia, and Pindos geotectonic units. The area in which the dam was constructed consists exclusively of flysch, the formation of Pindos unity.

The right (north) dam's abutment is characterized by low-grade formations due to intense tectonism. The left (south) abutment is dominated by sandstones (flysch sandstone phase), which are mainly medium-layered with thin intercalations of siltstone and are generally corrugated aspects of large scale.

2.2 Dam Description

The construction of Mornos Dam began in 1969. The dam is located in the Mornos River, about 220 km northwest of Athens, and is one of the largest earthen dams in Europe. The repletion of

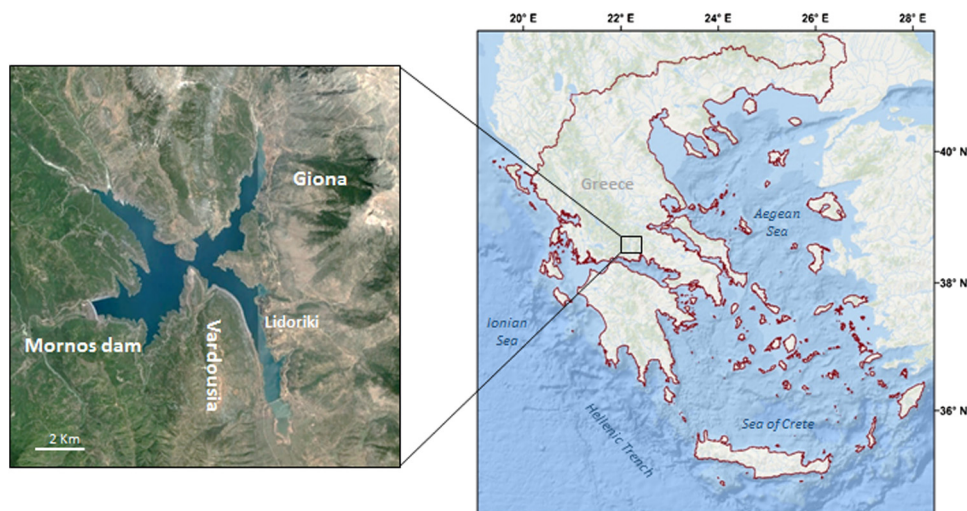


Fig. 1 Location map of the study area.

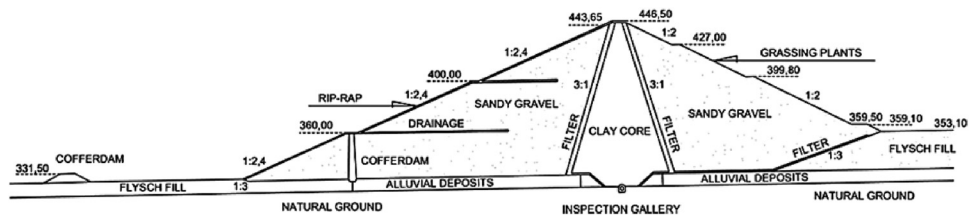


Fig. 2 Cross section of Mornos dam.⁴

the reservoir began in 1979, and all works were completed by 1981. It is a large earth dam with a medium-size central clay core. It is 126 m high, the crest length is 815 m, and its width from toe to toe is 660 m (Fig. 2).

The dam forms a man-made reservoir with surface area of 18.5 km² and watershed area of 560 km². Its maximum capacity is 764 million m³ of water, while its operational volume is 630 million m³. With the installation of pumping units, an additional 70 million m³ of water can be abstracted. The embankment component aggregates, which vary in size from sand particles to gravels, consist mainly of sedimentary (limestone, sandstone, and shale) rocks.⁵ The lake has a maximum depth exceeding 100 m and an average depth of 52 m.⁶ It consists of two sub-basins (Fig. 3) communicating through a narrow strait. Mornos River as well as a number of streams discharge into the lake.

3 Seismic Hazard of the Broader Area

In the surrounding area of the dam, several seismic events over 5.0 Mw [Figs. 4(a) and 4(b)] have occurred within the temporal range covered by this study.

3.1 June 1995 Aigion Earthquake

On June 15, 1995, an earthquake of moment magnitude 6.2 Mw occurred in the western part of the Gulf of Corinth, Greece [Fig. 4(a)], causing the loss of 26 human lives and inflicting considerable damage, mainly in the northern part of Peloponnesus. The earthquake was located according to the National Observatory of Athens ~12 km to the NNE of Aigion, under the northern coast of the gulf and 23 km SSE of Mornos Lake. The Harvard solution⁸ (Harvard,

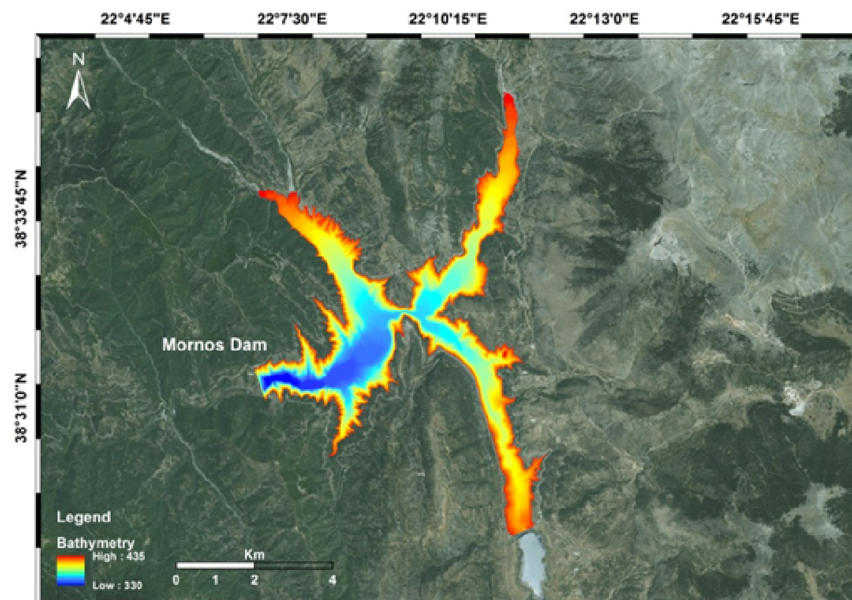


Fig. 3 Location area and bathymetry of Mornos reservoir.

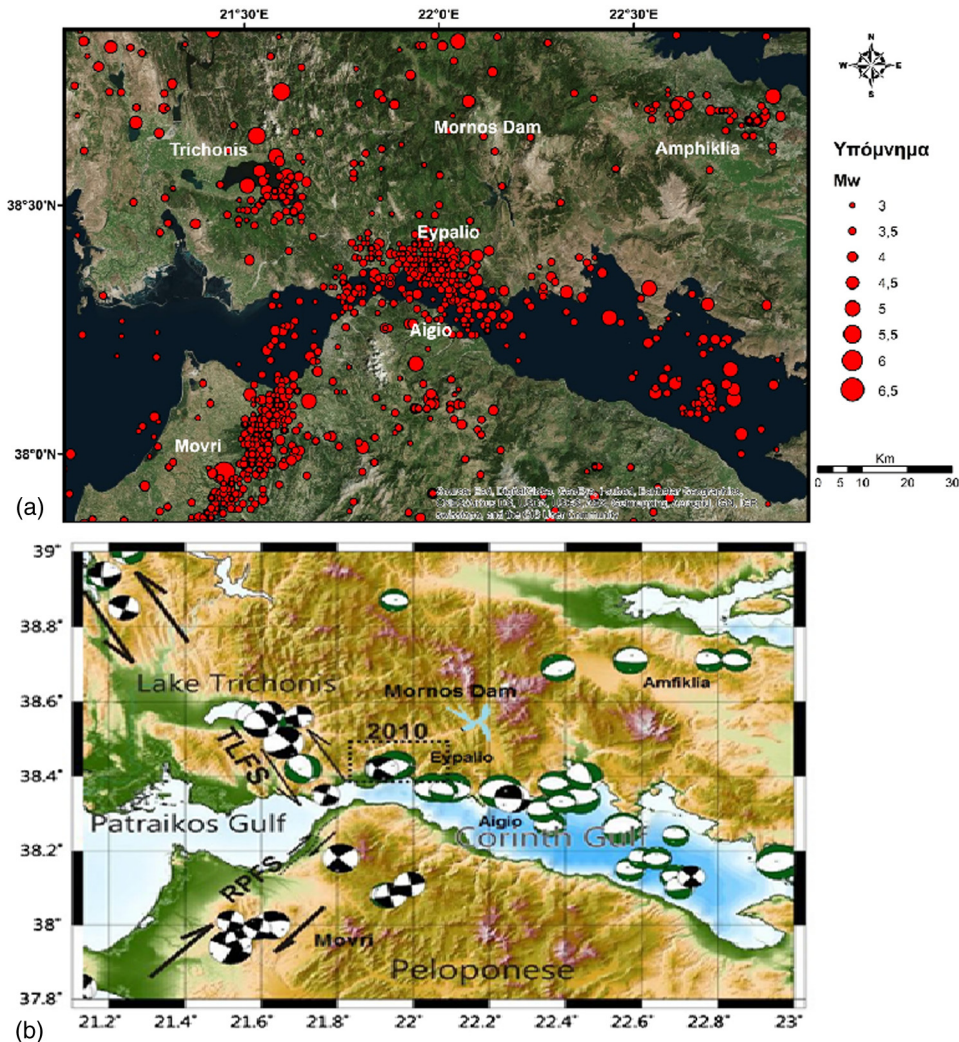


Fig. 4 (a) Location of epicenters of the main seismic events in a wide area (seismological data source: National Observatory of Athens) and (b) regional tectonic of a wide area and available earthquake focal mechanisms.⁷

1995) is an east–west striking, almost pure normal fault with a dip angle of 45 deg, and further more accurate studies have shown that this angle is most probably in the range of 30 to 35 deg.

3.2 April 2007 Trichonis Earthquake

During April 2007, a seismic swarm took place in the area of Trichonis Lake (W. Greece), 43 km west of Mornos Lake [Fig. 4(a)]. The swarm began with small events on April 9, and two days later, the three strongest events of the entire sequence occurred, with sizes ranging from 5.0 to 5.2 Mw located in the southeastern part of Trichonis Lake. The seismic activity continued for a month with smaller-magnitude events.^{9,10} This seismic activity was not correlated with any of the two fault zones at the northern and southern edges of the lake but with two unmapped NNE–SSW and NW–SE faults along its eastern shore.^{7,9,10}

3.3 June 2008 Movri Earthquake

On June 8, 2008, an earthquake of 6.4 Mw and depth 17.5 km struck NW Peloponnesus [Fig. 4(a)]. The epicenter was located in the wider Andravida area (Movri), 30 km SW from the city of Patras and 82 km SW of Mornos Lake. The horizontal deformation field was extended even far away the epicenter.¹¹ According to the moment tensor solutions for the earthquake

issued [National Observatory of Athens (NOA), HARV, INGV, USGS, ETHZ, AUTH] and the geographical distribution of its aftershocks, the fault strikes NE-SW and dips ~ 85 deg NW, while the motion was right-lateral with a small reverse component.¹² It was felt throughout Peloponnesus, in western Greece, and in Attica, and especially in the city and the suburbs of Patras. It triggered a number of landslides and rockfalls, toppled old buildings and poorly reinforced houses, and cracked reinforced concrete buildings in nearby communities. No evidence of surface rupture or significant surface deformation based on field work was observed.¹³

3.4 December 2008 Amfiklia Earthquake

On December 13, 2008, 08:27 GMT, an earthquake measuring 5.1 Mw occurred at ~ 10 km SE of the town of Lamia in central Greece [Fig. 4(a)], close to the small town of Amfiklia and 40 km NE of Mornos Lake. Despite its moderate magnitude, the earthquake caused minor damage (mostly cracks and plaster falls) in Amfiklia and nearby villages. Limited landslides were also observed, and as a consequence, traffic in one country road was interrupted for a few hours. Epicenters of this small sequence are gathered on top of the south-facing slope of the topographic high to the north of Amfiklia. Known large faults have been mapped to the north and dip to the north. In this frame, the 2008 sequence appears to be related to a small structure, antithetic to the known large faults, that bounds the Gravia–Amfiklia depression to the north.^{14,15}

3.5 January 2010 Efpalio Earthquake

On January 18, 2010, 15:56 UTC, a 5.1 Mw (NOA) earthquake occurred near the town of Efpalio (western Gulf of Corinth, Greece) [Fig. 4(a)], ~ 10 km to the east of Nafpaktos, along the north coast of the gulf and 20 km SSW of Mornos Dam. Another strong event occurred on January 22, 2010, 00:46 UTC, with 5.1 Mw (NOA) ~ 3 km to the NE of the first event. The two largest events were accompanied by a sequence of aftershocks, which lasted almost six months. Both M5+ shocks exhibited normal faulting along east–west trending planes. The first event ruptured a blind, north-dipping fault, accommodating north–south extension of the western Gulf of Corinth. The dip direction of the second event is rather unclear, although a south dip plane is weakly imaged in the post–January 22, 2010, aftershock distribution.⁷

4 Synthetic Aperture Radar Data Used and Interferometric Processing

In the present work, archived data from AMI and ASAR active sensors mounted on ERS-1 and 2 and ENVISAT satellites operated by the European Space Agency (ESA) were exploited for the interferometric analysis.

A total number of 128 single-look complex acquisitions of mode I2 (incidence angle ~ 23 deg), with VV polarization operating in the C-band, covering an area of 100 km by 100 km, were used. Among them, for the period of 1992 to 2000, a number of 20 ascending and 40 descending acquisitions were acquired by the AMI active sensor. Moreover, for the period of 2003 to 2010, a number of 29 ascending and 39 descending acquisitions were acquired from the ASAR active sensor. High accuracy orbital data from the DELFT Institute (NL) for Earth-Oriented Space Research¹⁶ were obtained for ERS-1 and 2 satellites. Moreover, high accuracy orbital data from the Doppler Orbitography and Radio-positioning Integrated by Satellite instrument were obtained for the ENVISAT satellite. The topographic phase was simulated based on SRTM V3 DEM of ~ 90 m spatial resolution.

In order to relate the pattern of the deformation with possible sources of deformations, seismological data for the period of 1992 to 2010 for the Mornos region and the wider area, which are available from the website of the European Mediterranean Seismological Centre and the Institute of Geodynamics, NOA, as well as data of the water level of the Mornos artificial lake given by the Athens Water Supply and Sewerage Company (EYDAP SA), were used.

In the present study, we have applied a multitemporal hybrid InSAR methodology, which combines elements from conventional DInSAR, satellite-based augmentation system,^{17,18} and

persistent scatterer interferometry (PSI). The immediate products of this procedure allow us to extract information of the displacements projected to the radar line of sight.^{16,19}

Due to the fact that the relief is rough and mountainous and the land cover is heavily vegetated and rural (with a lack of stable scatterers), we considered it more appropriate to use the SVD (hybrid InSAR) instead of the PSI approach. This way the produced map will have denser spatial coverage.

Moreover, to reveal the deformation history, the SVD method was also applied.¹⁸ The SVD method connects independent subsets of SAR acquisitions separated by large spatial baselines, thus increasing the amount of data used for the analysis of the area of interest (AOI).²⁰ Gamma processing software was used for processing and manipulating SAR data²¹ and ran in a Linux operating system.

Two separate processing procedures were carried out for AMI and ASAR data sets. All the interferometric pairs were multilooked by a factor of 1 in range and 5 in azimuth direction. The data set was coregistered to a single master scene, obtaining coregistration accuracies for the slaves <0.06 pixels in range and 0.2 pixels in azimuth. A subset of the full image frame was selected by cropping the coregistered scenes to the AOI.

The topographic component was removed to produce the differential interferograms (referred to as interferograms hereafter). The interferometric pairs are characterized by small spatial and temporal baselines in order to limit the noise components usually referred to as decorrelation phenomena.²² For the period of AMI acquisitions (1992 to 2000), spatial perpendicular baselines up to 300 m and temporal baselines up to three years for the ascending as well as up to 250 m and up to two years for the descending track were selected to form a sufficient network. For the period of ASAR acquisitions (2003 to 2010), spatial perpendicular baselines up to 300 m and temporal baselines up to three years for the ascending as well as up to 300 m and up to two years for the descending track were selected (Fig. 5). Particularly, 41 AMI interferograms were produced from the ascending and 134 from the descending track. Moreover, 71 ASAR interferograms were produced from the ascending and 171 from the descending track. Using a large volume of multireference differential interferograms, the temporal uncorrelated errors are reduced. Tropospheric turbulences, assumed to be uncorrelated in time, have been removed by visual interpretation. Moreover, tropospheric noise due to variable phase delay correlated with the altitude (stratification) as well as orbital fringes are also recognizable. For this reason, heavily suffering interferograms are removed. Therefore, the obtained time series of unwrapped phases could still include a small component of atmospheric phases as well as nonlinear deformation phase. The interferograms were further analyzed and filtered using adaptive filters.²³

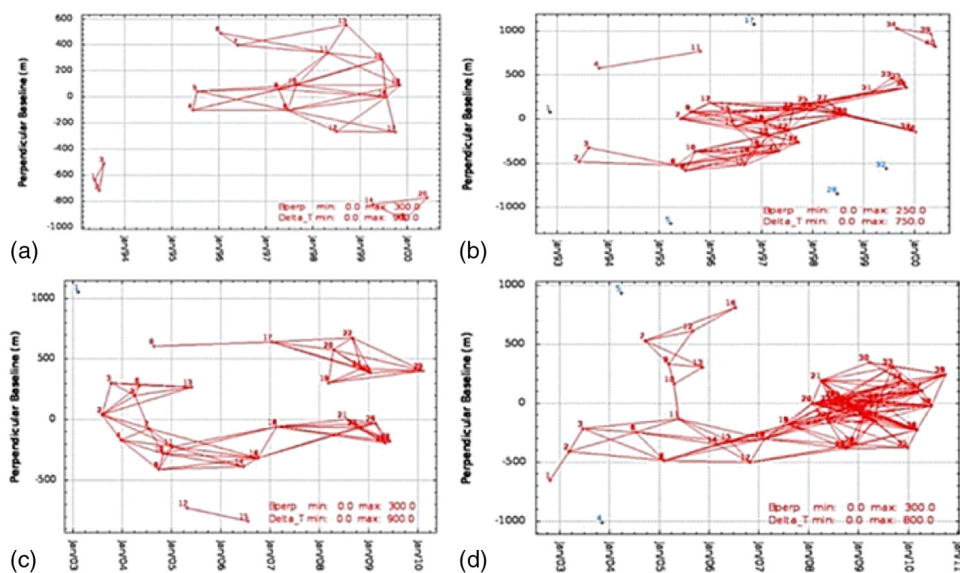


Fig. 5 (a) and (b) ERS scenes relating to the AMI ascending and descending data sets, respectively, and (c) and (d) ENVISAT scenes relating to the ASAR ascending and descending data sets.

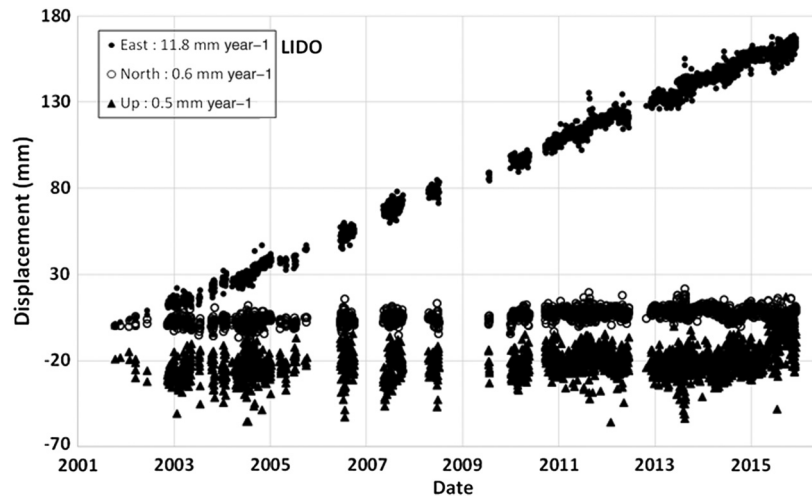


Fig. 6 Time series of the permanent Global Navigation Satellite System stations LIDO.

The interferograms were unwrapped using the minimum cost-flow algorithm.²⁴ The threshold for the average coherence was set to 0.3. The reference point was carefully selected in order to avoid biases, which can lead to shifts in the deformation patterns. It was located on stable ground 7 km ENE of the dam area, in Lidoriki village, near the LIDO permanent GPS station from the Corinth Rift Laboratory network.²⁵ The absolute velocities of LIDO in the ITRF2008 (Fig. 6) for east, north, and up components are 11.8, 0.6, and 0.5 mm year⁻¹, respectively.²⁵ The estimation of the temporal evolution of the deformation is calculated by using a weighted least-squares algorithm that minimizes the sum of squared weighted residual phases such as is provided from the SVD method.

5 Interferometric Results and Temporal Comparison with Relevant Seismic Events

The final products were projected to Universal Transverse Mercator zone 34N (WGS84) projection and superimposed over the shaded relief.

Due to the high slopes facing east–west, the coverages of the ascending and descending tracks are very different. For this reason, the decomposition is not possible for the whole Mornos Lake area as it is the case for the dam area. Thus, in the paragraphs following, we will investigate the spatial distribution of the deformations detected in the broader area with the two tracks side by side. The dam will be investigated for the horizontal and vertical velocities after the decomposition of the two tracks. Finally, the time series analysis will be performed only in the line of sight (LOS) velocities due to the different time slots between ascending and descending passes.

5.1 Temporal Ground Deformation for the Period of 1992 to 2000, During Active Microwave Instrument Acquisitions

The deformation maps of ascending [Fig. 7(a)] and descending [Fig. 7(b)] tracks as well as the time series deformation measurements for specific points on the dam are presented herein. In Fig. 7(a), it is indicated that generally the relative velocities toward and away from the satellite along the LOS varied between maximum values of +10 and -10 mm year⁻¹, respectively. Particularly, an area along the lake shore A across from Lidoriki village presents a deformation of +5 mm year⁻¹ toward the satellite, while higher toward the mountain Vardousia, a deformation of -2 mm year⁻¹ toward the satellite was measured. Moreover, there is an area at the Giona Mountain B where the deformation is up to -8 mm year⁻¹, and perhaps it is due to landslide phenomena. At the dam, the left (north) abutment seems stable with a slight deformation toward the dam in the range of +2 mm year⁻¹, while the right (south) abutment and the upstream side of the dam were considered stable.

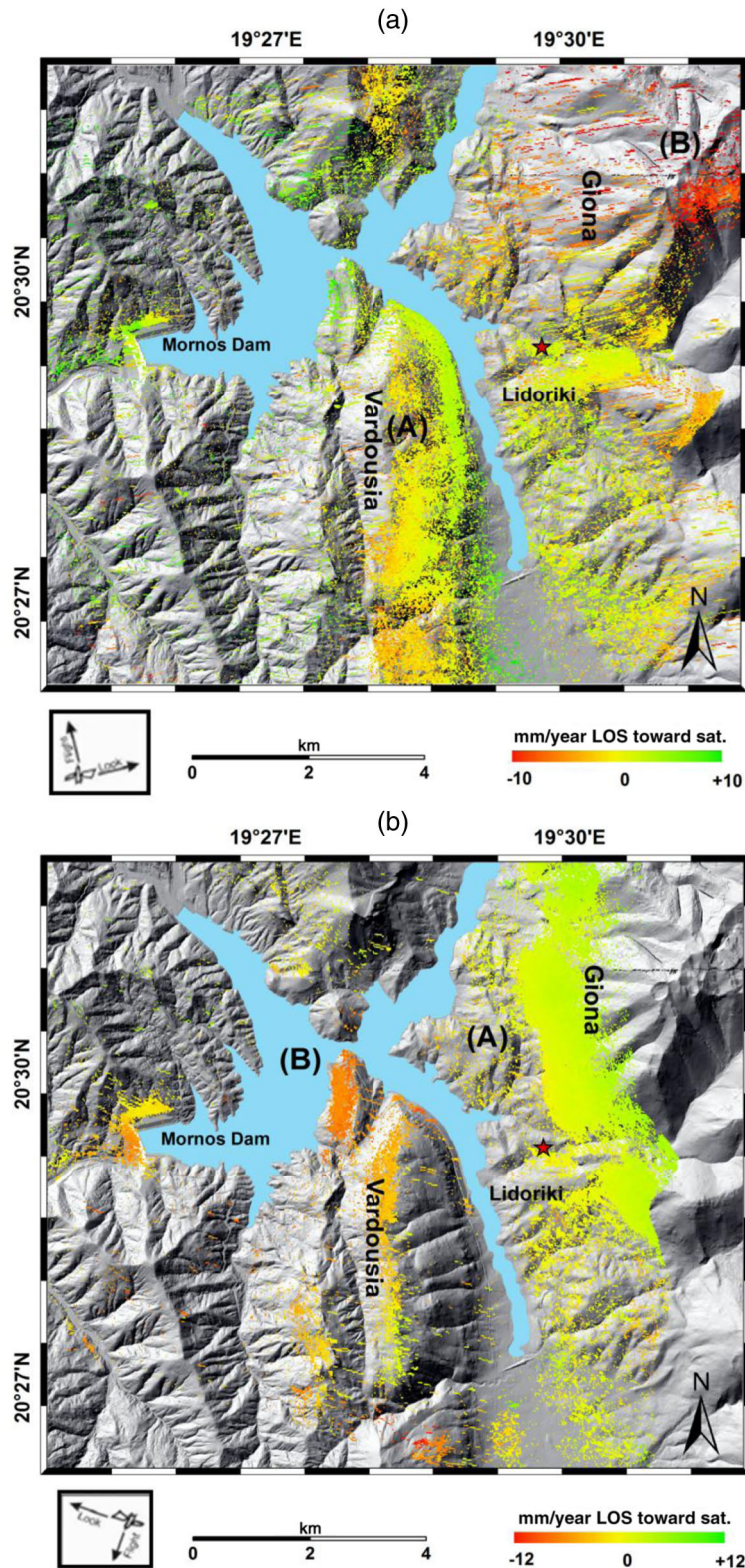


Fig. 7 (a) Hybrid InSAR LOS deformation rates for the period from 1992 to 2000 (sensor AMI/ERS-1 and 2, ascending track) and (b) hybrid InSAR LOS deformation rates for the period from 1992 to 2000 (sensor AMI/ERS-1 and 2, descending track). The location of the reference point is shown with a red star. Positive values represent deformation toward the satellite.

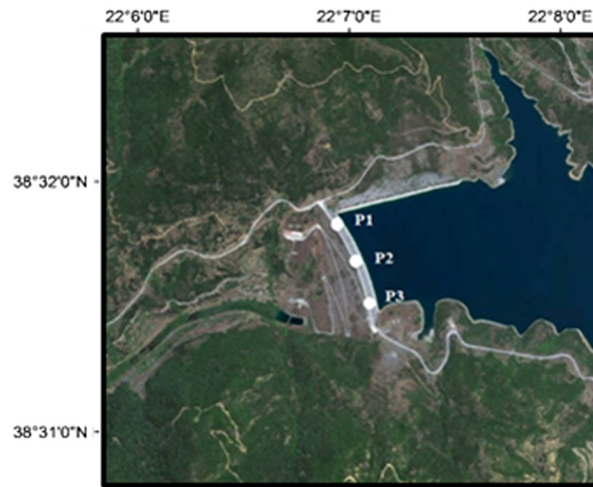


Fig. 8 Selected point targets on the downstream side of the dam.

In Fig. 7(b), the relative velocities toward and away from the satellite along the LOS varied between maximum values of $+12$ and -12 mm year^{-1} , respectively. Particularly, an area along the foothills of Giona Mountain A remains stable, but at higher altitudes, a deformation of about $+3$ to $+5$ mm year^{-1} toward the satellite is observed. Moreover, there is an area B at Vardousia Mountain presenting a deformation from -4 to -6 mm year^{-1} . Focusing on the area of the dam, both the abutments are characterized as stable with a small deformation of -1 mm year^{-1} , while the downstream side of the dam presents a deformation of -7 mm year^{-1} toward the satellite. Time series analysis diagrams by means of the hybrid InSAR time series method for specific point targets (Fig. 8) on the downstream side of the dam were plotted (Fig. 9). We selected the downstream side because of the orientation (westward) and the more coherent pixel, and this is because when the satellite travels in a descending orbit, it views a target area looking westward (in right-looking mode).

In Fig. 9, the deformation pattern of all points is similar. However, the deformation rate is directly related to the level of the artificial lake. During specific time periods when the level of the artificial lake is increasing, either because of rainfall or due to the water drained from Evinos Dam, the (Mornos) dam presents a negative deformation, while during periods when the level of the lake is reduced, the dam presents a positive deformation. However, during the period from June 3, 1995, to September 17, 1995 (indicated by black circle), the dam was expected to remain stable due to the constant level of the lake, but instead it presented a deformation of -3 cm overall. This effect was probably due to the strong Aigion earthquake (6.2 Mw) that occurred on June 15, 1995, which may have locally affected the response of the dam. The correlation between the level of the artificial lake and the deformation in the dam is ~ 0.66 .

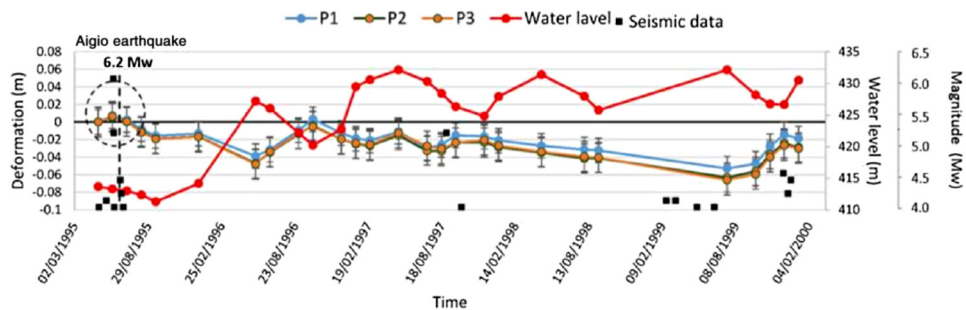


Fig. 9 Correlation of time series deformation (1995 to 2000), level of artificial lake, and seismic data at point targets on the Mornos Dam. The standard deviations (σ) of the deformation values are plotted as well. σ of P1, P2, and P3 are 0.014, 0.016, and 0.017 m, respectively.

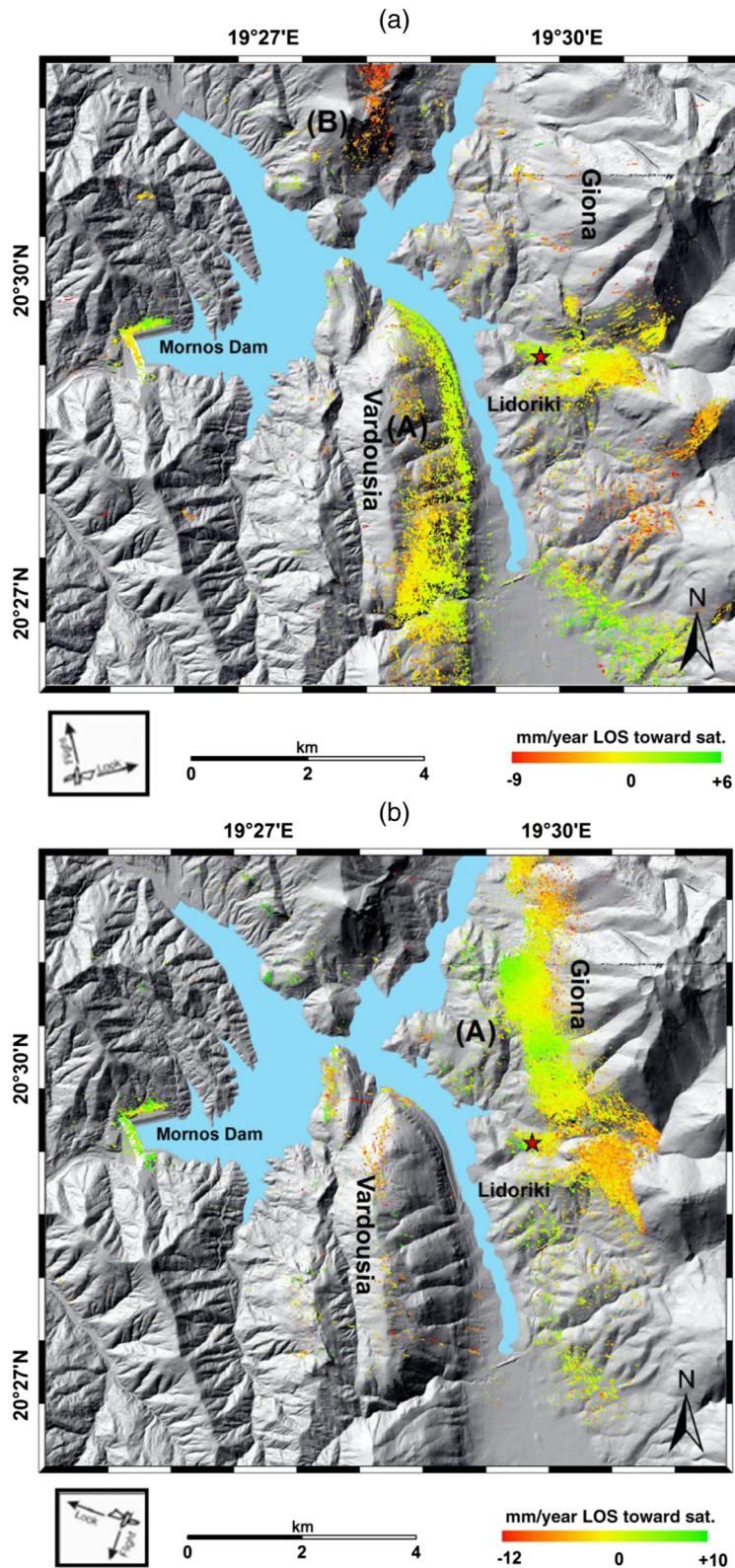


Fig. 10 (a) Hybrid InSAR LOS deformation rates for the period from 2003 to 2010 (sensor ASAR/ENVISAT, ascending track) and (b) hybrid InSAR LOS deformation rates for the period from 2003 to 2010 (sensor ASAR/ENVISAT, descending track). The location of the reference point is shown with a red star.

5.2 Temporal Ground Deformation for the Period from 2003 to 2010, During Advanced Synthetic Aperture Radar Acquisitions

The deformation maps of ascending [Fig. 10(a)] and descending [Fig. 10(b)] tracks as well as the time series deformation measurements for specific points on the dam (Fig. 8) are presented herein.

In Fig. 10(a), the relative vertical velocities toward and away from the satellite along its LOS varied between maximum values of $+6$ and -9 mm year^{-1} , respectively. Particularly, there is an area along the lake shore A across from Lidoriki village that presents a deformation of $+3$ mm year^{-1} toward the satellite, while higher toward the mountain Bardousia, the deformation is -1.5 mm year^{-1} . Furthermore, north of Bardousia, there is an area B with deformation of ~ -7 up to -9 mm year^{-1} . This may be due to landslide phenomena or neotectonic movements in the area. Focusing on the area of the dam, we observed that along the left (north) abutment, a dissimilar deformation existed with a deformation rate of -1 mm year^{-1} near the dam, a deformation of $+2.5$ mm year^{-1} at the middle of the abutment, and again a deformation of -1 mm yr^{-1} at the end. This was probably due to the different geological formation, which caused landslide phenomena. The right (south) abutment was characterized as stable, and the upstream side of the dam presented a deformation of -2 mm year^{-1} .

In Fig. 10(b), the relative velocities toward and away from the satellite along its LOS varied between maximum values of $+10$ and -12 mm year^{-1} , respectively. An area along the foothills of Giona Mountain A presents a deformation of $+2$ mm year^{-1} and in higher altitudes a deformation of about up to -5 mm year^{-1} toward the satellite. This may be due to tropospheric phenomena. Focusing on the area of the dam, the left (north) abutment had the same deformation pattern as in the ascending track, while the right (south) abutment presents a deformation of $+2$ mm year^{-1} . The downstream side of the dam presented a deformation of $+4$ mm year^{-1} toward the satellite. The deformation pattern was the same for all points (Fig. 11), and the deformation rate was related to the level of the artificial lake.

In periods where the lake level is increasing, the dam presents a negative deformation, and during the decrease of the level of the lake, the dam presents a positive deformation, respectively. However, during specific periods, this behavior did not take place. From February 11, 2007, to August 5, 2007 (left dashed circle), and from December 22, 2009, to October 3, 2010 (right dashed circle), the relationship of the deformation rate and the level of the lake was inverted. This effect might be correlated with the strong earthquakes that occurred on April 10, 2007, in Trichonis Lake (5.2 Mw) and on January 18, 2010, in Efpalio (5.3 Mw), locally affecting the response of the dam. However, further evidence is needed to confirm a direct link. A more remote and stronger earthquake occurred on June 8, 2008, in Movri (6.2 Mw), which did not affect the response of the dam. The correlation between the level of the artificial lake and the deformation in the dam is ~ 0.29 .

5.3 Decomposition of LOS Deformation

Due to the availability of both ascending and descending tracks, we could compute the east–west and vertical components as Ref. 20 proposed. The sensitivity of the deformation in the direction

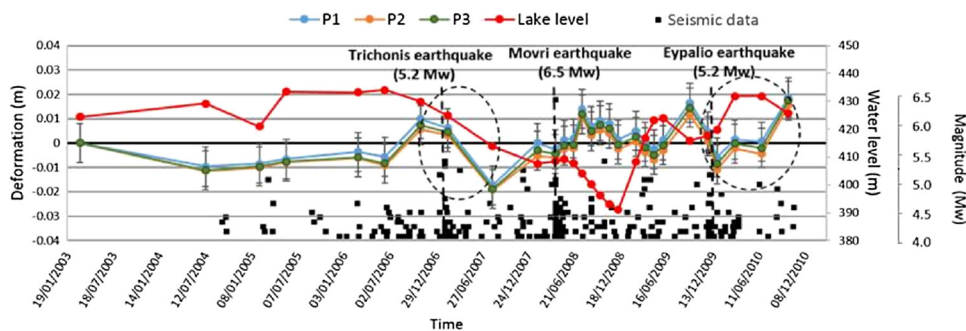


Fig. 11 Correlation of time series deformation (2003 to 2010), level of artificial lake, and seismic data at point targets on the Mornos Dam. The standard deviations (σ) of the deformation values are plotted as well. σ of P1, P2, and P3 are 0.008, 0.0075, and 0.0078 m, respectively.

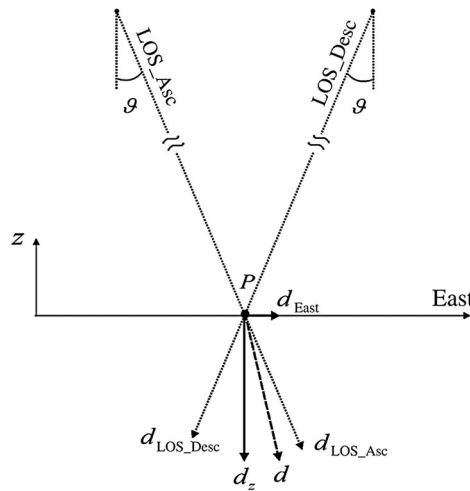


Fig. 12 SAR geometry in the east-z plane with the displacement vector \mathbf{d} (dashed line), its LOS projections $d_{\text{LOS_Asc}}$ and $d_{\text{LOS_Desc}}$ (dotted line), and the east-west and vertical deformation components d_{East} and d_z (continuous line) highlighted, respectively. A simplified ascending and descending radar geometry is considered here, wherein we assume parallel satellite tracks, orthogonal to the east-z plane.²⁰

parallel to the track of the satellite (heading) is zero, and since the angular distance with the north direction is very small (~ 13 deg), the north-south component could be assumed to be negligible. This investigation is focused only in the Mornos Dam, and Fig. 12 explains the basic rationale of this procedure.

5.3.1 Decomposition of LOS deformation, for period from 2003 to 2010, during advanced synthetic aperture radar acquisitions

This section presents the combination of ascending and descending deformation maps of advanced synthetic aperture radar, in order to retrieve the vertical [Fig. 13(a)] and east-west [Fig. 13(b)] components. This period was chosen due to the fact that the amount of ASAR acquisitions was more than that of AMI/ERS (1993 to 2000) as well as that in this period the seismicity in the broader area was higher.

In Fig. 13(a), the dam presents a uniform vertical deformation of ~ -4 mm year⁻¹; at the left (north) abutment, there is an area where the vertical deformation is ~ -7 mm year⁻¹, while the other part has the same rate as the dam. Probably, this area presents landslide phenomena. The right (south) abutment presents a uniform vertical deformation of ~ -8 mm year⁻¹.

Finally, in Fig. 13(b), the dam presents a uniform deformation of ~ 2 mm year⁻¹ to the west, while the left (north) abutment presents a differential horizontal deformation. The section near the dam and the end have a deformation of ~ 2 mm year⁻¹ to the east, while the middle part has a deformation of ~ 2 mm year⁻¹ to the west. The right (south) abutment presents a horizontal deformation to the east of the dam.

6 Discussion and Conclusion

In an effort to investigate potential earthquake-induced deformation to the Mornos earth dam (central Greece), we applied multitemporal SAR interferometry using AMI/ERS and ASAR/ENVISAT scenes, which together cover the period of 1993 to 2010.

In the present study, starting from the multireference stack of unwrapped phases, we derived a time series of deformation using SVD to obtain the least-squares solution for the phase time series. By using a large volume of multireference differential interferograms, the temporal uncorrelated errors were reduced. Tropospheric turbulences, assumed to be uncorrelated in time, were reduced in space. On the other hand, tropospheric noise due to variable phase delay linked to the

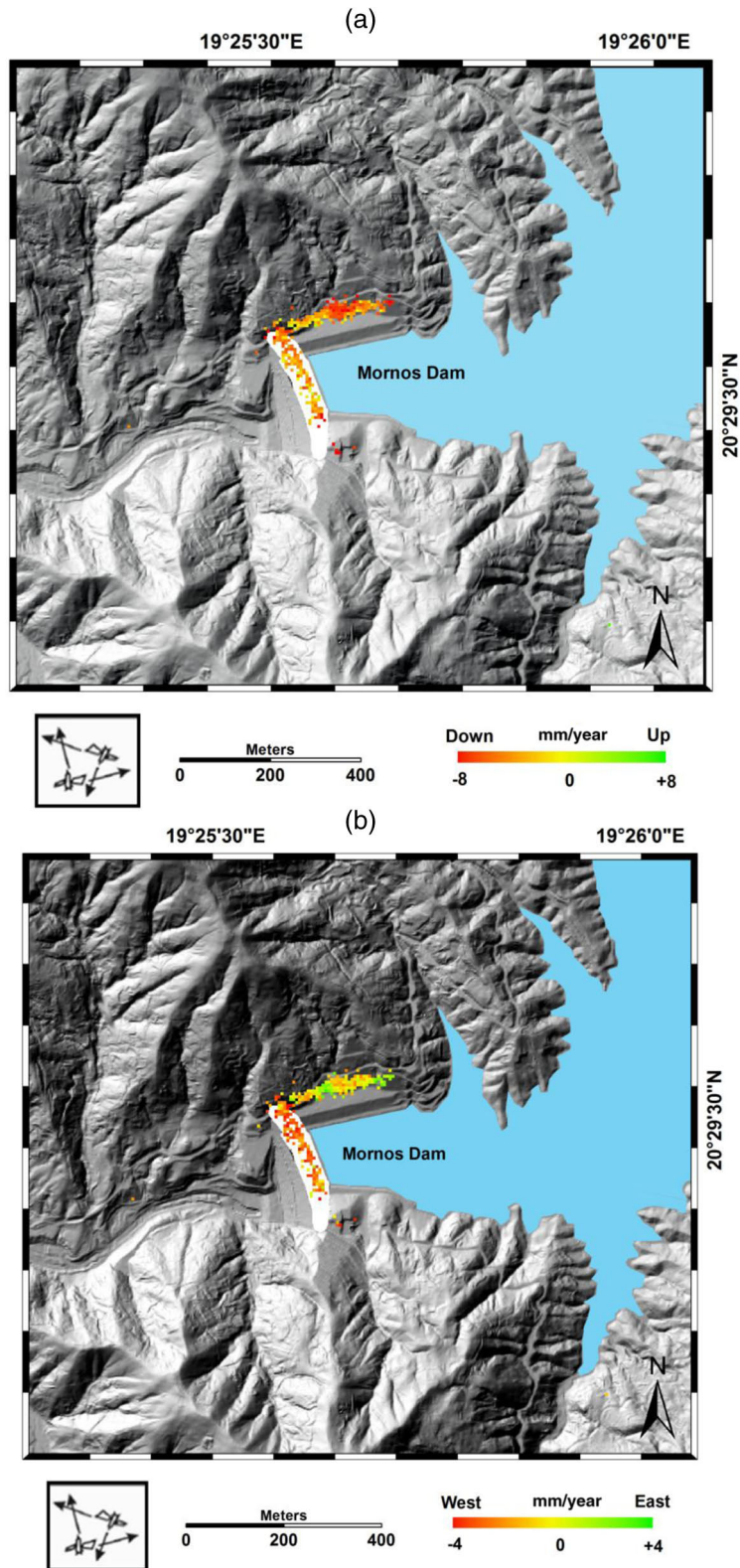


Fig. 13 (a) Hybrid InSAR UP component deformation rates for the period from 2003 to 2010 (satellite ENVISAT) and (b) hybrid InSAR EAST component deformation rates for the period from 2003 to 2010 (satellite ENVISAT).

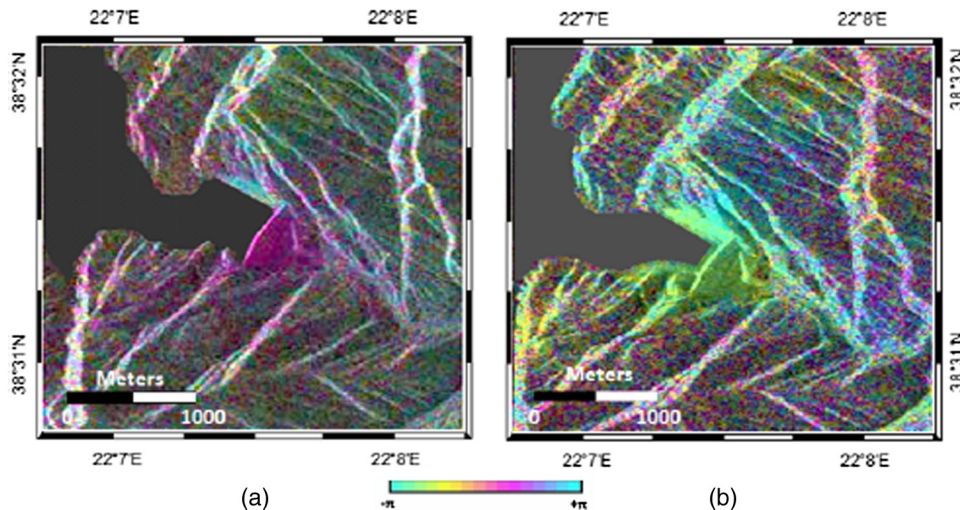


Fig. 14 (a) Interferometric pair 20091122–20100411 with Bp 80 m and Bt 140d during the earthquake of Eypalio (January 18 to January 22, 2010, $M_w = 5.3$) and (b) interferometric pair 20080127–20080615 with Bp 80 m and Bt 140d without seismic event.

altitude (smaller phase delay values in higher altitudes) is not reduced by this estimation procedure. For this reason, heavily suffering interferograms have been removed from the procedure. Tropospheric phases as well as phases relating to nonlinear motion are part of the deviation of the time series from the linear regression.²⁶

The products of multitemporal interferometric analysis are a time series of deformation history, temporally referenced to the date of the oldest acquisition (containing both the linear and nonlinear deformation components) and the (linear) deformation rate (velocity) for each scatterer. Nonlinear deformation can be estimated without any modeling and prior knowledge using the SVD as stated by Ref. 27. In order to have a numerical estimation of the statistical dependence between the water level and the deformation, we sampled the values of the water level at the acquisition dates and correlated them with the deformation values at the same dates. Thus, the resulting correlation value is an index of causation.

Results show that deformation measured by SAR interferometry is clearly related to water level changes but may also be associated with some of the earthquakes that struck the broader area during the period of monitoring. Three characteristic points that we considered and distributed along the crest of the dam show identical deformation behavior. Specifically, when the lake's level was increasing, the deformation is also increasing, and vice versa for the opposite case. This correlation ceases simultaneously with the event of some earthquakes that occurred in the region. This is evident by investigating inter-seismic and co-seismic interferometers (Fig. 14) presenting deformation between the dam crest and the abutments. This was not caused by atmospheric effects because the deformation does not behave as a large wavelength (smoothed) one but is abrupt. Furthermore, it is remarkable that the water-level variation through the period from 1995 to 2000 is up to 20 m and the maximum deformation rate is 6 cm. Instead, in the period from 2003 to 2010, the water-level variation is up to 40 m and the maximum deformation rate is 4 cm. This probably is due to the number of AMI/ERS acquisitions used, which are much less than the ones of ASAR/ENVISAT. Moreover, the qualities of the AMI sensor and AMI/ERS precise orbits are less than that of ASAR/ENVISAT.

The above findings are consistent with geodetic results carried out in Ref. 3. The authors used precise leveling and GPS measurements on the dam's crest for the period from 2002 to 2004. They also found a clear relation of dam behavior and variations in water volume in a seasonal scale. Unfortunately, during the period from 2002 to 2004, no important seismic event had occurred in the area, which could be recorded by the geodetic measurements.

As far as the border area of Mornos Dam is concerned, comparing the deformation pattern in ascending and descending tracks, the areas with similar spatial distribution, in which the deformation pattern is different, perhaps present a horizontal deformation.

The present study is important in that it provides that SAR interferometry can be used to monitor earth-dam behavior, in this case a study of Mornos Dam, as it is exposed to seismic hazard. The safety of infrastructures and the associated mitigating measures require a good knowledge of the causes of deformation. Future research should be directed to using very high spatial and temporal resolution radar data, that is, TerraSAR-X or Cosmo Sky Med, as well as to test more experimental interferometric processing.

Finally, the results of this case study certainly create the basis for further research with the contribution of seismologists and engineering geologists in investigating queries resulting such as why certain events have an effect and/or what their characteristics are.

Acknowledgments

The authors would like to thank European Space Agency for the AMI/ERS and ASAR/ENVISAT data through cat-1 6287 and Athens Water Supply and Sewerage Company (EYDAP SA) for the water level data of the Mornos artificial lake.

References

1. L. M. DeKay and H. G. McClelland, "Predicting loss of life in cases of dam failure and flash flood," *Risk Anal.* **13**(2), 193–205 (1993).
2. E. E. James et al., "Lessons from a dam failure," *Ohio J. Sci.* **100**(5), 121 (2000).
3. V. Gikas et al., *Deformation Studies of the Dam of Mornos Artificial Lake via Analysis of Geodetic Data FIG Working Week*, FIG, Cairo, Egypt (2005).
4. V. Gikas and M. Sakellatiou, "Settlement analysis of the Mornos earth dam (Greece): evidence from numerical modeling and geodetic monitoring," *Eng. Struct.* **30**(11), 3074–3081 (2008).
5. Lahmeyer International Consulting Engineers, "Mornos Dam: 780 million m³ reservoir for water supply to Athens area," Technical Report, Athens, Greece (1976).
6. I. A. Papadimitrakis and S. Karalis, "3-D water quality simulations in Mornos reservoir," *Global NEST J.* **11**(3), 298–307 (2009).
7. E. Sokos et al., "The April 2007 swarm in Trichonis Lake using data from a microseismic network," in *Proc. of the 12th Int. Congress Bulletin of the Geological Society of Greece*, Vol. XLIII, p. 2183 (2010).
8. P. Bernard et al., "The Ms = 6.2, June 15, 1995 Aigion earthquake (Greece): evidence for low angle normal faulting in the Corinth rift," *J. Seismol.* **1**, 131–150 (1997).
9. P. A. Evangelidis et al., "Waveform relocation and focal mechanism analysis of an earthquake swarm in Trichonis Lake, western Greece," *Bull. Seismol. Soc. Am.* **98**(2), 804–811 (2008).
10. A. Kiratzi et al., "The April 2007 earthquake swarm near Lake Trichonis and implications for active tectonics in western Greece," *Tectonophysics* **452**(1–4), 51–65 (2008).
11. A. Serpetsidaki et al., "New constraints from seismology and geodesy on the M_w = 6.4 2008 Movri (Greece) earthquake: evidence for a growing strike-slip fault system," *Geophys. J. Int.* **198**(3), 1373–1386 (2014).
12. G. Papadopoulos et al., "Crustal deformation associated with east Mediterranean strike-slip earthquake: the 8 June 2008 Movri (NW Peloponnese), Greece, earthquake (Mw 6.4)," *Tectonophysics* **492**(1–4), 201–212 (2010).
13. P. Briole et al., "Multidisciplinary study of the June 8, 2008, Mw = 6.4 Andravida earthquake," in *31st General Assembly, European Seismology Commission* (2008).
14. A. Ganas and I. Papoulia, "High-resolution, digital mapping of the seismic hazard within the Gulf of Evia rift, Central Greece using normal fault segments as line sources," *Nat. Hazards* **22**, 203–223 (2000).
15. P. G. Roberts and A. Ganas, "Fault-slip directions in central and southern Greece measured from striated and corrugated fault planes: comparison with focal mechanism and geodesy data," *J. Geophys. Res.* **105**, 23443–23462 (2000).
16. A. Gabriel, R. Goldstein, and H. Zebker, "Mapping small elevation changes over large areas by differential radar interferometry," *J. Geophys. Res.* **94**, 9183–9191 (1989).

17. S. Usai, "A least-squares approach for long-term monitoring of deformations with differential SAR interferometry," in *Proc. of the IEEE Int. Geoscience and Remote Sensing Symp.*, Vol. 2, pp. 1247–1250 (2002).
18. P. Berardino et al., "A new algorithm for surface deformation monitoring based on small baseline differential SAR interferograms," *IEEE Trans. Geosci. Remote Sens.* **40**, 2375–2383 (2002).
19. D. Massonnet et al., "The displacement field of the Landers earthquake mapped by radar interferometry," *Nature* **364**, 138–142 (1993).
20. M. Manzo et al., "Surface deformation analysis in the Ischia Island (Italy) based on spaceborne radar interferometry," *J. Volcanol. Geotherm. Res.* **151**(4), 399–416 (2005).
21. U. Wegmuller and C. Werner, "Gamma SAR processor and interferometry software," *Eur. Space Agency* **414**(3), 1687–1692 (1998).
22. H. A. Zebker and J. Villasenor, "Decorelation in interferometric radar echoes," *IEEE Trans. Geosci. Remote Sens.* **30**(5), 950–959 (1992).
23. R. M. Goldstein and C. L. Werner, "Radar interferogram filtering for geophysical applications," *Geophys. Res. Lett.* **25**(21), 4035–4038 (1998).
24. M. Constantini, "A novel phase unwrapping method based on networks programming," *IEEE Trans. Geosci. Remote Sens.* **36**(3), 813–821 (1998).
25. P. Elias and P. Briole, "Small scale ground deformations observed in the western rift of Corinth by exploiting multitemporal interferometry and GPS measurements," European Geosciences Union General Assembly 2014, 27 April–02 May, Vienna, Austria (2014).
26. S. Usai, "A least-squares approach for long-term monitoring of deformations with differential SAR interferometry," in *Proc. of the IEEE Int. Geoscience and Remote Sensing Symp.*, Vol. 2, pp. 1247–1250 (2002).
27. K. Goel, N. Adam, and C. Minet, "Long term analysis of strong non-linear deformations induced by coal mining using the SBAS technique," presented at *ESA Fringe Symp.*, 19–23 September 2011, Frascati, Italy (2011).

Spiros Neokosmidis received his BSc degree in geology and geoenvironment from the National and Kapodistrian University of Athens in 2012 and his MSc degree in geoinformatics from the Department of Geography of the Harokopio University of Athens in 2014. His current research interests include remote sensing, study of tectonic activity and ground deformation using SAR interferometric processing, and structural geology.

Panagiotis Elias has participated in research projects in the field of earth sciences as a space geodesy specialist, exploiting the synergy of remote sensing data and in-situ measurements aiming to the detection and measuring of the ground deformation and modelling its source as well as infrastructure instability due to geophysical processes or human-induced activities, respectively. He is also experienced in field campaigns.

Issaak Parcharidis is an associate professor of remote sensing at Harokopio University of Athens. He received his BSc in geological sciences from the University of Parma (Italy) and a PhD from the Agricultural University of Athens. He is the author of more than 30 journal papers and more than 80 papers in international conference proceedings. His current research interests include the use of SAR interferometry and high-resolution optical data for natural hazard assessment and disaster monitoring, and mitigation.

Pierre Briole is senior scientist at the French National Centre for Scientific Research (CNRS). He earned his PhD in 1990 at the Institut de Physique du Globe de Paris and since 2007 he is working at Ecole Normale Supérieure, Paris. He is expert in geodesy and remote sensing applied to volcanoes and seismic zones.